Light-assisted Néel spin currents in $\mathcal{PT}$-symmetric antiferromagnetic semiconductors

Shibo Fang,[1,*] Baochun Wu,[2,*] Qiuhui Li,[1] Zongmeng Yang,[1] Honglin Du,[1,3,4] Jinbo Yang,[1,3,4,5] Zhaochu Luo,[1,†] and Jing Lu[1,3,4,5,6,7,‡]

[1]*State Key Laboratory for Mesoscopic Physics and School of Physics, Peking University, Beijing 100871, People's Republic of China*
[2]*State Key Laboratory of Low Dimensional Quantum Physics and Department of Physics, Tsinghua University, Beijing 100871, People's Republic of China*
[3]*Collaborative Innovation Center of Quantum Matter, Beijing 100871, People's Republic of China*
[4]*Beijing Key Laboratory for Magnetoelectric Materials and Devices (BKL-MEMD), Peking University, Beijing 100871, People's Republic of China*
[5]*Peking University Yangtze Delta Institute of Optoelectronics, Nantong 226010, People's Republic of China*
[6]*Key Laboratory for the Physics and Chemistry of Nanodevices, Peking University, Beijing 100871, People's Republic of China*
[7]*Beijing Key Laboratory of Quantum Devices, Peking University, Beijing 100871, People's Republic of China*

(Received 21 October 2023; revised 9 January 2024; accepted 22 January 2024; published 13 February 2024)

Néel spin current is defined as the staggered spin current across different magnetic sublattices and can manipulate the Néel vector of the antiferromagnet by its associated spin-transfer torques. Currently, it is believed that Néel spin currents are only generated through electrical driving in $\mathcal{PT}$-symmetric antiferromagnetic metals, which is a linear effect. In this paper, we propose that Néel spin currents can be induced through the nonlinear optical effect (spin photogalvanic effect) in $\mathcal{PT}$-symmetric antiferromagnetic semiconductors. Using CrSBr and CrI_3 as representatives, we predict that light can generate Néel spin current in antiferromagnetic semiconductors, with both staggered and antiparallel spin currents distributed across different magnetic sublattices, depending on the $\mathcal{PT}$ symmetries of their corresponding spin photogalvanic coefficients. We show that the origin of the diverse manifestations of light-assisted Néel spin currents lies in the nonlinearity of the spin photogalvanic effect, resulting in the current not necessarily being the staggered spin current. Our work proposes a nonlinear effect that may have tremendous application potential in future antiferromagnetic devices.

DOI: 10.1103/PhysRevB.109.085201

I. INTRODUCTION

Antiferromagnets possess several advantages over ferromagnets, including ultrafast terahertz (THz) spin dynamics, robustness against external magnetic perturbations, and the absence of stray fields, which makes antiferromagnets highly promising for next-generation highly integrated and ultrafast memory devices [1–3]. Ferromagnetic memory devices achieve storage functionality by controlling the relative alignment of magnetic moments between two separate ferromagnetic electrodes [4,5]. Unlike ferromagnetic memories, the functionality of antiferromagnetic (AFM) memory relies on the manipulation of the Néel vector ($\boldsymbol{M}_{\mathrm{Ne'el}}$), which is defined as $\boldsymbol{M}_{\mathrm{Ne'el}} = \boldsymbol{M}_1 - \boldsymbol{M}_2$ ($\boldsymbol{M}_1$ and $\boldsymbol{M}_2$ represent the magnetic moments of the first and second sublattices, respectively) [6]. Controlling the relative orientation of Néel vectors enables the realization of tunneling magnetoresistance (TMR) effect in tunnel junctions composed of the antiferromagnetic metals [7]. Furthermore, the modulation of Néel vector is of significant importance for exploring novel physical phenomena such as the hidden spin polarization [8,9] and spin-neutral tunneling anomalous Hall effect [2].

Recently, Shao *et al.* proposed that due to symmetry constraints, the spin currents from different magnetic sublattices in $\mathcal{PT}$-symmetric AFM systems are opposite in spin but of equal magnitude [Fig. 1(a)] [10]. They referred to this staggered spin current as the Néel spin current for it can reverse the Néel vector through the spin-transfer torque (STT) effect [11]. When applying a bias voltage to AFM metals, the Néel spin current manifests as two spin-polarized currents with the same transport direction but opposite spin orientations [Fig. 1(b)]. However, this definition holds true only when the $\mathcal{PT}$ symmetry of the spin-polarized current ($J_{\mathrm{up/down}}$) is even, i.e., $\mathcal{PT}$ $J_{\mathrm{up}} = J_{\mathrm{down}}$ (up and down refers to different spin orientations). If the spin-polarized current possesses other $\mathcal{PT}$ symmetry types (e.g., $\mathcal{PT}$ odd), the manifestation of the defined Néel spin current will be completely different [12–14]. For example, when the spin-polarized currents are $\mathcal{PT}$ odd, the resulting Néel spin current manifests as two counterpropagating spin-polarized currents, distributed on different sublattices, with opposite spin and transport directions. In this paper, we refer to such a Néel spin current as the "antiparallel spin current." The antiparallel spin current carries the same angular momentum for different sublattices, leading to a tendency for antiferromagnetic order to transform into the ferromagnetic order [10,15].

In semiconductors, it is challenging to excite Néel spin currents electrically due to its poor conductivity, whereas the optical or thermal assistance are more desirable [16,17].

*These authors contributed equally to this work.
†Corresponding author: jinglu@pku.edu.cn
‡Corresponding author: zhaochu.luo@pku.edu.cn

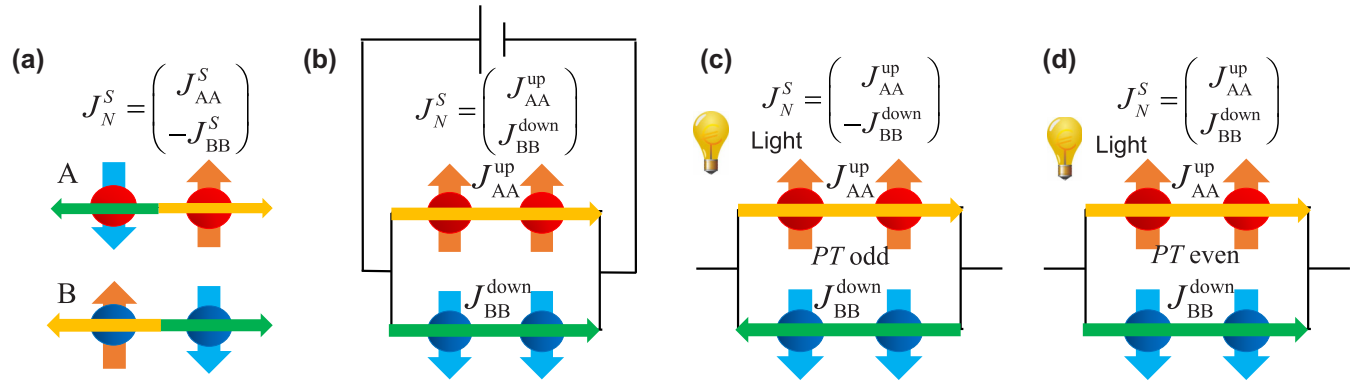

FIG. 1. (a) Schematic diagram of the Néel spin current J_N^S. A (red ball) and B (blue ball) denote the atoms in different magnetic sublattices. J_{AA} and J_{BB} correspond to the currents flowing through the AA and BB sublattices, respectively. The orange upward and blue downward arrows indicate the spin up and down, respectively. The horizontal yellow and green arrows represent the flow directions of spin-up and spin-down polarized currents, respectively. J_N^S in the $\mathcal{PT}$-symmetric AFM semiconductors under (b), electrical driving and optical excitation with the spin photogalvanic coefficients being $\mathcal{PT}$ (c) odd and (d) even.

For instance, the photogalvanic effect and spin photogalvanic effect allow for the generation of charge current and spin current in semiconductor systems, respectively [15,18–22]. Recently, research on photogalvanic effect and spin photogalvanic effect in $\mathcal{PT}$-symmetric AFM semiconductors has gained increasing attention. For example, Xiao *et al.* and Fei *et al.* proposed that the pure spin current can be generated by the linear shift current [13] and circular injection current [12] in $\mathcal{PT}$-symmetric AFM systems, respectively. However, the spatial distribution characteristics of that pure spin current excited in $\mathcal{PT}$-symmetric AFM semiconductors have not yet been studied. Whether such spin currents can be classified as the Néel spin current remains unknown.

In this work, we propose the light-assisted Néel spin current in the $\mathcal{PT}$-symmetric semiconductors. We define the extended global Néel spin current as a binary vector consisting of staggered spin currents from different magnetic sublattices [Eq. (1) and Fig. 1(a)], with their respective basis vectors corresponding to different magnetic sublattices. Our definition consists with Shao's definition for the electric-assisted systems [11]. By employing *ab initio* quantum transport simulations, we investigate the electric current and photocurrent in bilayer CrSBr and CrI_3 antiferromagnetic tunnel junctions (AFMTJs). Under electrical assistance, the CrSBr AFMTJ can excite Néel spin currents composed of the staggered spin current across different magnetic sublattices [Fig. 1(b)]. Under optical excitation, the CrSBr and CrI_3 AFMTJs can excite both the antiparallel [Fig. 1(c)] and the staggered spin current [Fig. 1(d)] across different magnetic sublattices, which is determined by the corresponding $\mathcal{PT}$ symmetries of the spin photogalvanic effect. In the presence of mirror symmetry protection, the photocurrent manifests as only the antiparallel spin current irrespective of the incident light [Fig. 1(c)], which is totally different with the case in the $\mathcal{PT}$-symmetric AFM metals.

II. NÉEL SPIN CURRENT IN AFM SEMICONDUCTORS

We consider a collinear AFM semiconductor that consists of two magnetic sublattices A and B with negligible spin-orbit coupling. The intrasublattice distance d_{AA} is always smaller than the intersublattice distance d_{AB} in the studied systems, indicating that the currents generated in these two sublattices are spatially separated and satisfy the criteria for Néel spin currents [11]. Hence, we assume that the current flowing through the same sublattice ($J_{AA/BB}$) dominates and neglect the influence of the current flowing through different sublattices (J_{AB}). J and $J^s (J^s = J^{up} - J^{down})$ denote the magnitudes of the charge currents and spin currents, respectively. Here, we define the Néel spin current J_N^S as a binary vector with their respective basis vectors corresponding to the spin current of different magnetic sublattices:

$$J_N^S = \begin{pmatrix} J_{AA}^S \\ -J_{BB}^S \end{pmatrix}, \tag{1}$$

where the positive and negative signs here refer to different flowing directions, and the first and second dimensions represent the spin currents flowing through in the sublattice AA and BB, respectively. Here, we have assigned a negative sign to the spin current in the second sublattice for the purpose of consistency with the previous definition in AFM metals. However, the actual direction of the spin flow in the second sublattice needs to be determined through further calculations.

When a bias electrical field $\boldsymbol{E}$ is applied to the AFM semiconductor with a finite thickness, an electrical current would be generated, where the current is a first-order response to the electric field [23]. By using the linear response theory, the real part of the frequency (ω)-dependent electrical conductivity $\sigma_{\boldsymbol{E}}^{\alpha}(\omega)$ with spin α in the Bloch system is [24]

$$\sigma_{\boldsymbol{E}}^{\alpha}(\omega) = \frac{\mu}{\omega} \int \sum_{m,n} (f_m - f_n) \langle m|v_\alpha(k)|n\rangle \times \langle n|v_\alpha(k)|m\rangle \delta(\varepsilon_{mn} - \hbar\omega) dk, \tag{2}$$

where m, n label the band index with ε_m, ε_n the corresponding eigenvalues and the associated Fermi-Dirac occupation numbers $f(\varepsilon_m)$, $f(\varepsilon_n)$.$\varepsilon_{mn} = \varepsilon_m - \varepsilon_n$ and $\Delta f_{mn} = f(\varepsilon_m) - f(\varepsilon_n)$. k is the wave vector, v_α the velocity operator with spin α, and μ the constant coefficient. After the $\mathcal{PT}$ transformation, the spin-dependent conductivity coefficient only causes a change in the spin orientation, i.e.,$\mathcal{PT}\sigma_{\boldsymbol{E}}^{\alpha}(\omega) = \sigma_{\boldsymbol{E}}^{-\alpha}(\omega)$. Due to the

presence of only one type of spin-polarized current in the A and B lattices, respectively, under the influence of an electric field, these spin-polarized currents will all move in a directed manner towards one direction. We can derive the electric-assisted Néel spin current:

$$J_N^S = \begin{pmatrix} J_{AA}^{\text{up}} \\ J_{BB}^{\text{down}} \end{pmatrix}. \tag{3}$$

It shows that the electrically driven Néel spin currents are globally spin-neutral currents consisting of two spatially separated and oppositely spin-polarized currents with the same transport direction [Fig. 1(b)], which is consistent with the previous works [10,11].

When the AFM semiconductor is illuminated uniformly with a light, a photocurrent is induced by the photogalvanic effect, which is the second-order response to the electric field $J_c^\alpha = \eta_{abc}^\alpha E_a E_b$ (a, b, and c are spatial coordinates). There are four types of photogalvanic effect coefficients: the linear shift current, linear injection current, circular shift current, and circular injection current (see details in the Supplemental Material [61]). The "linear" and "circular" correspond to linearly polarized and circularly polarized light excitations, respectively. The "injection" and "shift" correspond to the diagonal and off-diagonal elements of the nonequilibrium density matrix. Unlike the first-order response to the electric field, the coefficients of the second-order response to the electric field are not necessarily $\mathcal{PT}$ even. For example, the response coefficient of the circular injection current is [12]

$$\begin{aligned}\eta_{abc}^\alpha(\omega) = -\frac{\lambda}{\omega^2}\int \sum_{m,n} \text{Im}\left[v_{mn}^{\alpha,a}(k) v_{nm}^{\alpha,b}(k)\right] f_{mn} \\ \times \left(\langle m|\{\sigma_\alpha, v_c(k)\}|m\rangle \tau_m - \langle n|\{\sigma_\alpha, v_c(k)\}|n\rangle \tau_n\right) \\ \times \delta(\varepsilon_{mn} - \hbar\omega) dk,\end{aligned} \tag{4}$$

where λ is the constant coefficient,$v_{mn}^{\alpha,a}$ and $v_{mn}^{\alpha,b}$ are the a-direction and b-direction interband velocity matrix elements between the mth and nth states with α spin, respectively. Im is taking the imaginary part of the function, and $\{\cdot\}$ is the anticommutation operator. τ_m is the minimum value of spin-relaxation and free-carrier relaxation times of the mth band carrier. Since there is an imaginary term ($\mathcal{PT}$ odd) present in η_{abc}^α, while the other terms are $\mathcal{PT}$ even, the overall coefficient is $\mathcal{PT}$ odd, i.e.,$\mathcal{PT} J_{AA}^{\text{up}} = -J_{BB}^{\text{down}}$. This leads to the generation of currents with opposite spin orientations and transport directions on different sublattices [Fig. 1(c)]:

$$J_N^S = \begin{pmatrix} J_{AA}^{\text{up}} \\ -J_{BB}^{\text{down}} \end{pmatrix}. \tag{5}$$

As shown in Table I, the spin photogalvanic coefficients of the linear-polarized shift current (LPS) and circular-polarized injection current (CPI) are both $\mathcal{PT}$ odd [12–14], and the corresponding Néel spin currents are depicted in Fig. 1(c). While for the linear-polarized injection current (LPI) and circular-polarized shift current (CPS; $\mathcal{PT}$ even) [18], the Néel spin currents are depicted in Fig. 1(d). Without loss of generality, we choose the A-type AFM semiconductors CrSBr and CrI_3 to illustrate our theory (the calculation details of the bilayer AFM CrSBr and CrI_3 are shown in the Supplemental Material).

TABLE I. Mechanisms of photogalvanic effect for the charge current and spin current generation in $\mathcal{PT}$- symmetric AFM semiconductors. LPI, LPS, CPI, and CPS are the linear-polarized injection current, linear-polarized shift current, circular-polarized injection current, and circular-polarized shift current, respectively. "√" and "×" refer to nonzero and zero, respectively.

Mechanism	LPI	LPS	CPI	CPS
Spin current	×	√	√	×
Charge current	√	×	×	√
$\mathcal{PT}$ symmetry	Even	Odd	Odd	Even

In terms of manipulating the Néel magnetic moments, the $\mathcal{PT}$-odd terms inject the same amount of angular momentum into both sublattices, resembling a pure spin current but without time-reversal symmetry [62]. This leads to a transition from antiferromagnetic order to ferromagnetic order [4]. On the other hand, the $\mathcal{PT}$-even terms generate Néel spin currents that induce the rotation of the antiferromagnetic Néel vectors [11].

III. ELECTRIC-ASSISTED NÉEL SPIN CURRENTS

We design a lateral bilayer (BL) CrSBr AFMTJ based on a two-probe model and investigate its electrical transport properties by using density functional theory (DFT) coupled with the nonequilibrium Green's function (NEGF) method (see details in the Supplemental Material). As shown in Fig. 2(a), the device consists of the electrodes and channel, with the channel being the intrinsic CrSBr and the electrodes being the doped metallic CrSBr. The Néel vector of the source (left electrode) is kept along the $+z$ axis. When calculating the STT, the Néel vector of the drain (right electrode) is set along the y axis. As shown in Fig. 2(b), the STTs at $V_g = 0$ V in the different layers have opposite directions but the same magnitudes. This implies that the spin orientations of the current entering the drain from different layers exhibit exact antiparallel alignment, resulting in the emergence of a globally spin-neutral current across different sublattices. Such Néel spin currents are confirmed by the spin-resolved transmission eigenstates [Fig. 2(d) and Fig. S6 for the antiparallel (AP) state [61]]. When calculating the magnetoresistance, the Néel vector of the drain (right electrode) is set along the $+z$ and the $-z$ axis, corresponding to the parallel (P) and the AP states, respectively. The calculated AFM TMR reaches the considerable value of $\sim 8 \times 10^5$% (Table II), which is much larger than the calculated TMR (~500%) of the spin valve based on the ferromagnetic monolayer Fe_3GeTe_2 magnetic tunnel junction [63].

We subsequently investigated the Stark effect of this device to investigate the spatial distribution of the current. As V_g increases from 0 to 5 V, the transmission of spin-up electrons at the Fermi surface gradually rises, while that of the spin-down electrons gradually decreases, as shown in Fig. S7 [61]. When V_g reaches a threshold of 5 V, the spin-up channel becomes conductive [Fig. S8(c) [61]], and the spin-down

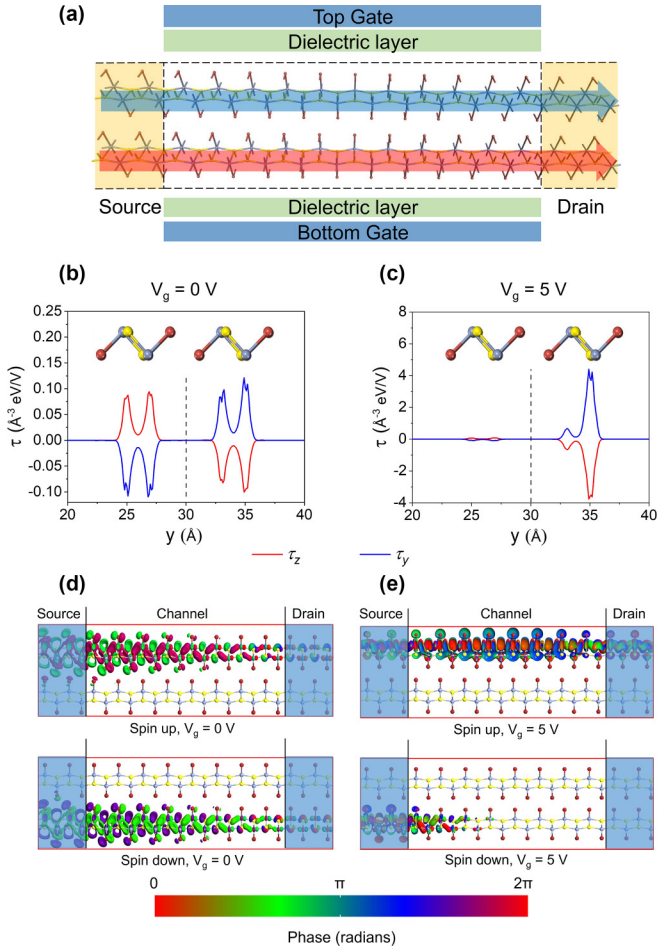

FIG. 2. (a) Schematic diagram of the electrically driven Néel spin current in the BL CrSBr AFM tunneling junction. Distribution of the z and y components of spin-transfer torkance τ in the drain of the bilayer CrSBr AFM tunneling junction at gate voltages $V_g =$ (b) 0 and (c) 5 V. The spin angle between the left and right electrodes is 90° when calculating τ. Spin-resolved transmission eigenstates for $V_g =$ (d) 0 and (e) 5 V. $k_{||} = (0.07, 0)$ and $(0.46, 0)$, isovalue $= 0.05$ and $0.1\,\text{Å}^{-3/2}\,\text{eV}^{-1/2}$ for (d) and (e), respectively. The value and the color of the isosurface represent the amplitude and the phase of the electron wave function, respectively.

channel remains insulated [Fig. S8(d) [61]]. Here, the STT and spin-polarized current are locally concentrated in the top layer, indicating that only the magnetic moments in the top layer are modulated, as shown in Figs. 2(c) and 2(e). Moreover, the current in the device is no longer a tunneling current and primarily exists in the upper layer, and the average STT of the conducting current ($V_g = 5$ V) is one order of magnitude larger than that of the tunneling current ($V_g = 0$ V). A spin-polarized current is produced with the spin polarization of 88% under zero bias voltage. As the bias voltage increases, the polarizability of the spin also gradually rises (reaching 92% at 3 V bias voltage; Fig. S9 [61]) and the magnetoresistance is up to $\sim 5 \times 10^5$% for $V_g = 5$ V (Table II). Our results shows that the electrically driven Néel spin current is layer distributed, and that the Stark effect can generate the spin current that only exists in a single layer.

IV. LIGHT-ASSISTED NÉEL SPIN CURRENTS

The photocurrent of the BL AFM CrSBr photodetector is also simulated by the DFT+NEGF method [51,53]. The photodetector, as shown in Fig. 3(a), shares the identical device configuration of the AFMTJ in Fig. 2(a). Upon illumination of the central region of the device, the photocurrent is generated and subsequently collected by the electrodes. According to the previous results of the Stark effect, the energy bands of bilayer AFM CrSBr can be regarded as a superposition of two oppositely ferromagnetic (FM) monolayers. We calculated the spin-resolved in-plane optical absorption tensors xx and yy of the monolayer FM CrSBr with opposite magnetic orders, as shown in Figs. 3(b) and 3(c). We find that the upper layer of CrSBr primarily absorbs photons to generate spin-up photocarriers, while the lower layer generates the spin-down photocurrent. This implies that the spin-polarized current generated in this device is layer distributed, exhibiting typical characteristics of the Néel spin current.

In the bilayer AFM CrSBr photodetector, due to the mirror (glide) reflection M_z along the transport direction z in the device, the total charge photocurrent of the device is constrained to be 0, i.e., $I_{\text{up}} + I_{\text{down}} = 0$ [15]. The photocurrent corresponding to $\mathcal{PT}$-even terms can only remain to be $0 (I_{\text{up}} = I_{\text{down}} = 0)$, while the photocurrent corresponding to $\mathcal{PT}$-odd terms can maintain $I_{\text{up}} = -I_{\text{down}}$ without necessarily being 0. Hence, the Néel spin photocurrents manifest as a pure spin current across different magnetic sublattices, which we name "antiparallel spin current." When the linearly [Fig. 3(a)] or right-handed circularly [Fig. 3(b)] polarized light is vertically incident, the spin-up (R_{up}) and spin-down (R_{down}) photocurrents exhibit a reverse direction with equal magnitudes, irrespective of the photon energy E. When E is fixed (e.g., $E = 1.3$ eV), changing the polarization angle θ and ϕ or the rotation angle α and β does not alter this relationship (the definitions of the above angles are shown in the Supplemental Material), as shown in Figs. S10(a)–S10(d) [61]. Namely, the generated Néel spin currents are robust against the incident

TABLE II. Calculated spin-dependent electron transmission $t_\uparrow$ and $t_\downarrow$ in CrSBr antiferromagnetic tunnel junction at different V_g. The Néel vector angle between the two electrodes is 0° and 180° in the parallel and antiparallel states, respectively. The calculation detail of the tunnel magnetoresistance (TMR) is provided in the Supplemental Material.

Gate voltage	Configuration	$t_\uparrow$	$t\downarrow$	t_{sum}	TMR
$V_g = 0$ V	Parallel	1.66×10^{-2}	1.66×10^{-2}	3.32×10^{-2}	835000%
	Antiparallel	1.52×10^{-6}	2.46×10^{-6}	3.97×10^{-6}	
$V_g = 5$ V	Parallel	2.92×10^{-1}	1.55×10^{-2}	3.08×10^{-1}	520000%
	Antiparallel	5.27×10^{-5}	6.45×10^{-6}	5.92×10^{-5}	

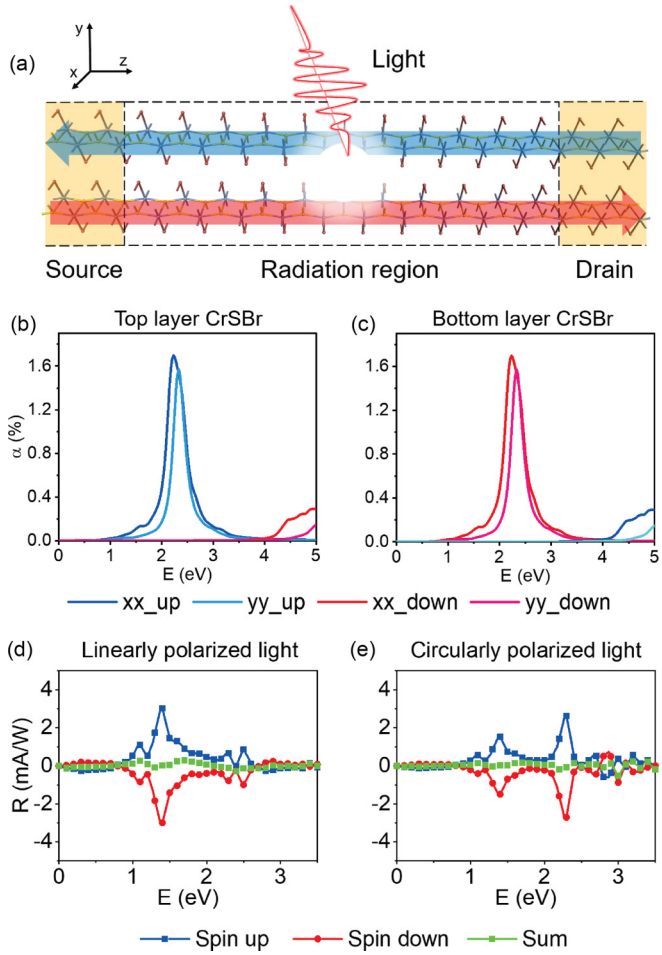

FIG. 3. (a) Schematic diagram of the light-assisted Néel spin current in bilayer AFM CrSBr photodetector. The blue and red arrows denote the spin-up and spin-down polarized current, respectively. Spin-resolved optical absorbance tensor of the (b) top and (c) bottom CrSBr monolayers, respectively. Spin-resolved photoresponse as a function of the photon energy E in the bilayer antiferromagnetic CrSBr photodetector under the (d) linearly polarized light and (e) right-handed circularly polarized light.

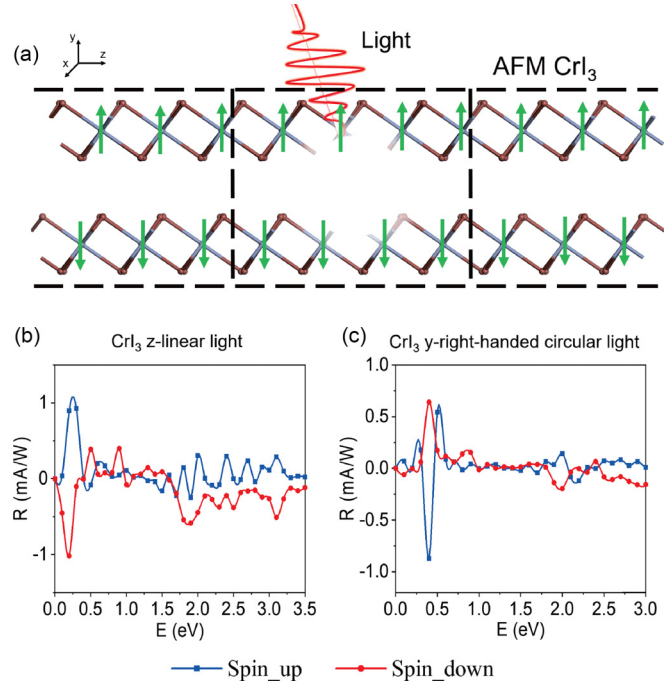

FIG. 4. (a) Schematic diagram of the antiferromagnetic CrI_3 photodetector. Spin-polarized photocurrent (light-assisted Néel spin current) of the antiferromagnetic CrI_3 under the (b) z linearly polarized light and (c) y right-handed circularly polarized light.

light. When changing the polarization and incident angles, the photocurrent exhibits a trigonometric function relationship with the angle, consistent with the photogalvanic effect observed in the experiments [64]. Note that there are still some small net charge photoresponses ($R_{\rm sum} = R_{\rm up} + R_{\rm down}$) under certain photon energies and polarizing angles. As shown in Table I, those net charge currents come from linear injection and circular shift currents. The reason is that the M_z only approximately holds in the CrSBr photodetector due to the difference between the NEGF with the perturbation theory (see details in the Supplemental Material). The maximum spin photoresponse ($R_s = R_{\rm up} - R_{\rm down}$) under the linear-polarized light is 6 mA/W at $E = 1.4$ eV, and that under the circularly polarized light is as large as 6 mA/W at $E = 2.3$ eV. Such photoresponse is comparable with the common theoretical values in two-dimensional van der Waals material based p-n junctions (e.g., 16.8 and 13.6 mA/W in monolayer Bi_2O_2Se and Bi_2O_2Te p-n junctions [65]). In addition, it can generate spin current in infrared and visible light regions, making it widely applicable for practical use [17].

When the mirror reflection symmetry is broken, the generated spin photocurrent will include both $\mathcal{PT}$-even and $\mathcal{PT}$-odd terms. To illustrate this point, we calculate the spin-dependent photocurrent in the A-type antiferromagnetic bilayer CrI_3, which also possesses $\mathcal{PT}$ symmetry but the broken $\mathcal{P}$ and $\mathcal{T}$ symmetries [26]. Here we investigate its photocurrent transportation in the absence of the mirror reflection symmetry M_z, as shown in Fig. 4(a). We find that under both (b), linearly polarized, and (c), circularly polarized light irradiation, the generated photocurrent is not like the antiparallel spin current in bilayer AFM CrSBr, as shown in Fig. 3. This is because the loss of mirror reflection symmetry leads to the generation of the $\mathcal{PT}$-even spin photocurrent. In this case, the Néel spin currents generated by the $\mathcal{PT}$-even terms have opposite spin directions but the same transmission direction, which is the staggered spin current and corresponds to Fig. 1(d). The photocurrent in this case is contributed by both the $\mathcal{PT}$-even and the $\mathcal{PT}$-odd terms.

Differing from the $\mathcal{PT}$-even terms, it is difficult to eliminate the $\mathcal{PT}$-odd terms through selecting specific symmetries [66]. In other words, when illuminating a $\mathcal{PT}$-symmetric antiferromagnetic system with light, it is challenging to generate only the staggered spin currents as the electric-assisted Néel spin currents. This is because the $\mathcal{PT}$-odd photocurrents are generated through either the linearly shifted current or the circularly injected current, with the primary physical quantities that control its symmetry being the Berry connection and the Berry curvature, respectively [19,67]. If we want both of these physical quantities to be zero, the system must

simultaneously possess $\mathcal{T}$ and $\mathcal{P}$ inversion symmetry, which contradicts our assumption. Therefore, in the systems with the $\mathcal{PT}$-symmetric and broken $\mathcal{P}$ and $\mathcal{T}$ symmetries, the light-assisted Néel spin currents can only exist in two forms: either the purely antiparallel spin currents or a combination of the antiparallel and staggered spin currents.

V. CONCLUSION

In this work, we extend the generation method of the Néel spin current from the electric-assisted $\mathcal{PT}$-symmetric metals to light-assisted $\mathcal{PT}$-symmetric semiconductors. The light-assisted Néel spin currents consist of the staggered or antiparallel spin currents distributed across different magnetic sublattices, depending on the $\mathcal{PT}$ symmetries of its corresponding spin photogalvanic coefficients. We show that the origin of the diverse manifestations of light-assisted Néel spin currents in semiconductors lies in the nonlinearity of the photogalvanic effect, resulting in the current not necessarily being $\mathcal{PT}$ even. Taking CrSBr and CrI_3 as examples, we verify the aforementioned theory through first-principles calculation combined with the quantum transport approach. Our work provides a path for utilizing optoelectronic methods to write in AFM memories.

ACKNOWLEDGMENTS

This work was supported by the Ministry of Science and Technology of China (Grants No. 2022YFA1203904 and No. 2017YFA206303), the National Natural Science Foundation of China (Grants No. 12241401, No. 91964101, and No. 12274002), the Fundamental Research Funds for the Central Universities, the High-Performance Computing Platform of Peking University, and the MatCloud+ high-throughput materials simulation engine.

The authors declare no conflict of interest.

[1] A. Du, D. Zhu, K. Cao, Z. Zhang, Z. Guo, K. Shi, D. Xiong, R. Xiao, W. Cai, J. Yin, S. Lu, C. Zhang, Y. Zhang, S. Luo, A. Fert, and W. Zhao, Electrical manipulation and detection of antiferromagnetism in magnetic tunnel junctions, Nat. Electron. **6**, 425 (2023).

[2] D.-F. Shao, S.-H. Zhang, R.-C. Xiao, Z.-A. Wang, W. J. Lu, Y. P. Sun, and E. Y. Tsymbal, Spin-neutral tunneling anomalous Hall effect, Phys. Rev. B **106**, L180404 (2022).

[3] V. Baltz, A. Manchon, M. Tsoi, T. Moriyama, T. Ono, and Y. Tserkovnyak, Antiferromagnetic spintronics, Rev. Mod. Phys. **90**, 015005 (2018).

[4] B. Wu, S. Fang, J. Yang, S. Liu, Y. Peng, Q. Li, Z. Lin, J. Shi, W. Yang, Z. Luo, C. Wang, J. Yang, J. Lu, and H. Du, High-performance Fe_xGeTe_2-based ($x = 4$ or 5) van der Waals magnetic tunnel junctions, Phys. Rev. Appl. **19**, 024037 (2023).

[5] P. Liu, J. Li, J. Han, X. Wan, and Q. Liu, Spin-group symmetry in magnetic materials with negligible spin-orbit coupling, Phys. Rev. X **12**, 021016 (2022).

[6] P. Němec, M. Fiebig, T. Kampfrath, and A. V. Kimel, Antiferromagnetic opto-spintronics, Nat. Phys. **14**, 229 (2018).

[7] J. Dong, X. Li, G. Gurung, M. Zhu, P. Zhang, F. Zheng, E. Y. Tsymbal, and J. Zhang, Tunneling magnetoresistance in non-collinear antiferromagnetic tunnel junctions, Phys. Rev. Lett. **128**, 197201 (2022).

[8] X. Zhang, Q. Liu, J.-W. Luo, A. J. Freeman, and A. Zunger, Hidden spin polarization in inversion-symmetric bulk crystals, Nat. Phys. **10**, 387 (2014).

[9] W. Chen, M. Gu, J. Li, P. Wang, and Q. Liu, Role of hidden spin polarization in nonreciprocal transport of antiferromagnets, Phys. Rev. Lett. **129**, 276601 (2022).

[10] D. F. Shao, S. H. Zhang, M. Li, C. B. Eom, and E. Y. Tsymbal, Spin-neutral currents for spintronics, Nat. Commun. **12**, 7061 (2021).

[11] D. F. Shao, Y. Y. Jiang, J. Ding, S. H. Zhang, Z. A. Wang, R. C. Xiao, G. Gurung, W. J. Lu, Y. P. Sun, and E. Y. Tsymbal, Néel spin currents in antiferromagnets, Phys. Rev. Lett. **130**, 216702 (2023).

[12] R. Fei, W. Song, L. Pusey-Nazzaro, and L. Yang, *PT*-symmetry-enabled spin circular photogalvanic effect in antiferromagnetic insulators, Phys. Rev. Lett. **127**, 207402 (2021).

[13] R.-C. Xiao, D.-F. Shao, Y.-H. Li, and H. Jiang, Spin photogalvanic effect in two-dimensional collinear antiferromagnets, npj Quantum Mater. **6**, 35 (2021).

[14] S. M. Young, F. Zheng, and A. M. Rappe, Prediction of a linear spin bulk photovoltaic effect in antiferromagnets, Phys. Rev. Lett. **110**, 057201 (2013).

[15] H. Xu, H. Wang, J. Zhou, and J. Li, Pure spin photocurrent in non-centrosymmetric crystals: Bulk spin photovoltaic effect, Nat. Commun. **12**, 4330 (2021).

[16] G. E. Bauer, E. Saitoh, and B. J. van Wees, Spin caloritronics, Nat. Mater. **11**, 391 (2012).

[17] M. Long, P. Wang, H. Fang, and W. Hu, Progress, challenges, and opportunities for 2D material based photodetectors, Adv. Funct. Mater. **29**, 1803807 (2018).

[18] Z. Dai and A. M. Rappe, Recent progress in the theory of bulk photovoltaic effect, Chem. Phys. Rev. **4**, 011303 (2023).

[19] R. Fei, X. Lu, and L. Yang, Intrinsic spin photogalvanic effect in nonmagnetic insulator, arXiv:2006.10690.

[20] J.-M. Lihm and C.-H. Park, Comprehensive theory of second-order spin photocurrents, Phys. Rev. B **105**, 045201 (2022).

[21] X. Jiang, L. Kang, J. Wang, and B. Huang, Giant bulk electrophotovoltaic effect in heteronodal-line systems, Phys. Rev. Lett. **130**, 256902 (2023).

[22] R. Fei, S. Yu, Y. Lu, L. Zhu, and L. Yang, Switchable enhanced spin photocurrent in Rashba and cubic Dresselhaus ferroelectric semiconductors, Nano Lett. **21**, 2265 (2021).

[23] S. Smidstrup *et al.*, QuantumATK: An integrated platform of electronic and atomic-scale modelling tools, J. Phys.: Condens. Matter **32**, 015901 (2020).

[24] L. Calderín, V. V. Karasiev, and S. B. Trickey, Kubo–Greenwood electrical conductivity formulation and implementation for projector augmented wave datasets, Comput. Phys. Commun. **221**, 118 (2017).

[25] B. Wu, J. Yang, S. Liu, S. Fang, Z. Liu, Z. Lin, J. Shi, W. Yang, Z. Luo, C. Wang, H. Du, J. Yang, and J. Lu, Layer-dependent magnetoresistance and spin-transfer torque in $MnSe_2$-based magnetic tunnel junctions, Phys. Rev. Appl. **19**, 064008 (2023).

[26] B. Wu, J. Yang, R. Quhe, S. Liu, C. Yang, Q. Li, J. Ma, Y. Peng, S. Fang, J. Shi, J. Yang, J. Lu, and H. Du, Scaling behavior of magnetoresistance with the layer number in CrI_3 magnetic tunnel junctions, Phys. Rev. Appl. **17**, 034030 (2022).

[27] Y. Wang, X. Xu, X. Zhao, W. Ji, Q. Cao, S. Li, and Y. Li, Switchable half-metallicity in A-type antiferromagnetic NiI_2 bilayer coupled with ferroelectric In_2Se_3, npj Comput. Mater. **8**, 218 (2022).

[28] Y. J. Bae, J. Wang, A. Scheie, J. Xu, D. G. Chica, G. M. Diederich, J. Cenker, M. E. Ziebel, Y. Bai, H. Ren, C. R. Dean, M. Delor, X. Xu, X. Roy, A. D. Kent, and X. Zhu, Exciton-coupled coherent magnons in a 2D semiconductor, Nature (London) **609**, 282 (2022).

[29] K. Yang, G. Wang, L. Liu, D. Lu, and H. Wu, Triaxial magnetic anisotropy in the two-dimensional ferromagnetic semiconductor CrSBr, Phys. Rev. B **104**, 144416 (2021).

[30] J. Yang, S. Fang, Y. Peng, S. Liu, B. Wu, R. Quhe, S. Ding, C. Yang, J. Ma, B. Shi, L. Xu, X. Sun, G. Tian, C. Wang, J. Shi, J. Lu, and J. Yang, Layer-dependent giant magnetoresistance in two-dimensional $CrPS_4$ magnetic tunnel junctions, Phys. Rev. Appl. **16**, 024011 (2021).

[31] N. P. Wilson, K. Lee, J. Cenker, K. Xie, A. H. Dismukes, E. J. Telford, J. Fonseca, S. Sivakumar, C. Dean, T. Cao, X. Roy, X. Xu, and X. Zhu, Interlayer electronic coupling on demand in a 2D magnetic semiconductor, Nat. Mater. **20**, 1657 (2021).

[32] Y. Wang, S. Liu, Q. Li, R. Quhe, C. Yang, Y. Guo, X. Zhang, Y. Pan, J. Li, H. Zhang, L. Xu, B. Shi, H. Tang, Y. Li, J. Yang, Z. Zhang, L. Xiao, F. Pan, and J. Lu, Schottky barrier heights in two-dimensional field-effect transistors: From theory to experiment, Rep. Prog. Phys. **84**, 056501 (2021).

[33] V. Wang, N. Xu, J.-C. Liu, G. Tang, and W.-T. Geng, VASPKIT: A user-friendly interface facilitating high-throughput computing and analysis using VASP code, Comput. Phys. Commun. **267**, 108033 (2021).

[34] M. Stamenova, P. Stamenov, F. Mahfouzi, Q. Sun, N. Kioussis, and S. Sanvito, Spin transfer torque in Mn_3Ga-based ferrimagnetic tunnel junctions from first principles, Phys. Rev. B **103**, 094403 (2021).

[35] R. Quhe *et al.*, Sub-10 nm two-dimensional transistors: Theory and experiment, Phys. Rep. **938**, 1 (2021).

[36] H. Lv, Y. Niu, X. Wu, and J. Yang, Electric-field tunable magnetism in van der Waals bilayers with A-type antiferromagnetic order: Unipolar versus bipolar magnetic semiconductor, Nano Lett. **21**, 7050 (2021).

[37] K. Lee, A. H. Dismukes, E. J. Telford, R. A. Wiscons, J. Wang, X. Xu, C. Nuckolls, C. R. Dean, X. Roy, and X. Zhu, Magnetic order and symmetry in the 2D semiconductor CrSBr, Nano Lett. **21**, 3511 (2021).

[38] R. K. Ghosh, A. Jose, and G. Kumari, Intrinsic spin-dynamical properties of two-dimensional half-metallic FeX_2 (X = Cl, Br, I) ferromagnets: Insight from density functional theory calculations, Phys. Rev. B **103**, 054409 (2021).

[39] B. Wu, R. Quhe, J. Yang, S. Liu, J. Shi, J. Lu, and H. Du, High-performance spin filters and spin field effect transistors based on bilayer VSe_2, Adv. Theory Simul. **4**, 2000238 (2020).

[40] J. Tong, F. Luo, L. Ruan, G. Qin, L. Zhou, F. Tian, and X. Zhang, High and reversible spin polarization in a collinear antiferromagnet, Appl. Phys. Rev. **7**, 031405 (2020).

[41] E. J. Telford, A. H. Dismukes, K. Lee, M. Cheng, A. Wieteska, A. K. Bartholomew, Y. S. Chen, X. Xu, A. N. Pasupathy, X. Zhu, C. R. Dean, and X. Roy, Layered antiferromagnetism induces large negative magnetoresistance in the van der Waals semiconductor CrSBr, Adv. Mater. **32**, e2003240 (2020).

[42] S. R. Singamaneni, L. M. Martinez, J. Niklas, O. G. Poluektov, R. Yadav, M. Pizzochero, O. V. Yazyev, and M. A. McGuire, Light induced electron spin resonance properties of van der Waals CrX_3 (X = Cl, I) crystals, Appl. Phys. Lett. **117**, 082406 (2020).

[43] Y. Peng, S. Ding, M. Cheng, Q. Hu, J. Yang, F. Wang, M. Xue, Z. Liu, Z. Lin, M. Avdeev, Y. Hou, W. Yang, Y. Zheng, and J. Yang, Magnetic structure and metamagnetic transitions in the van der Waals antiferromagnet $CrPS_4$, Adv. Mater. **32**, e2001200 (2020).

[44] H. Liu, X. Wang, J. Wu, Y. Chen, J. Wan, R. Wen, J. Yang, Y. Liu, Z. Song, and L. Xie, Vapor deposition of magnetic van der Waals NiI_2 crystals, ACS Nano **14**, 10544 (2020).

[45] R. Fei, W. Song, and L. Yang, Giant photogalvanic effect and second-harmonic generation in magnetic axion insulators, Phys. Rev. B **102**, 035440 (2020).

[46] T. Zhang, Y. Wang, H. Li, F. Zhong, J. Shi, M. Wu, Z. Sun, W. Shen, B. Wei, W. Hu, X. Liu, L. Huang, C. Hu, Z. Wang, C. Jiang, S. Yang, Q. M. Zhang, and Z. Qu, Magnetism and optical anisotropy in van der Waals antiferromagnetic insulator CrOCl, ACS Nano **13**, 11353 (2019).

[47] V. Kumar Gudelli and G.-Y. Guo, Magnetism and magneto-optical effects in bulk and few-layer CrI_3: A theoretical GGA $+ U$ study, New J. Phys. **21**, 053012 (2019).

[48] S. J. Gong, C. Gong, Y. Y. Sun, W. Y. Tong, C. G. Duan, J. H. Chu, and X. Zhang, Electrically induced 2D half-metallic antiferromagnets and spin field effect transistors, Proc. Natl. Acad. Sci. USA **115**, 8511 (2018).

[49] M. Stamenova, R. Mohebbi, J. Seyed-Yazdi, I. Rungger, and S. Sanvito, First-principles spin-transfer torque in CuMnAs|GaP|CuMnAs junctions, Phys. Rev. B **95**, 060403(R) (2017).

[50] B. Huang, G. Clark, E. Navarro-Moratalla, D. R. Klein, R. Cheng, K. L. Seyler, D. Zhong, E. Schmidgall, M. A. McGuire, D. H. Cobden, W. Yao, D. Xiao, P. Jarillo-Herrero, and X. Xu, Layer-dependent ferromagnetism in a van der Waals crystal down to the monolayer limit, Nature (London) **546**, 270 (2017).

[51] L. Zhang, K. Gong, J. Chen, L. Liu, Y. Zhu, D. Xiao, and H. Guo, Generation and transport of valley-polarized current in transition-metal dichalcogenides, Phys. Rev. B **90**, 195428 (2014).

[52] S. M. Young and A. M. Rappe, First principles calculation of the shift current photovoltaic effect in ferroelectrics, Phys. Rev. Lett. **109**, 116601 (2012).

[53] J. Chen, Y. Hu, and H. Guo, First-principles analysis of photocurrent in graphene P N junctions, Phys. Rev. B **85**, 155441 (2012).

[54] S. Grimme, J. Antony, S. Ehrlich, and H. Krieg, A consistent and accurate *ab initio* parametrization of density functional dispersion correction (DFT-D) for the 94 elements H-Pu, J. Chem. Phys. **132**, 154104 (2010).

[55] M. Brandbyge, J.-L. Mozos, P. Ordejón, J. Taylor, and K. Stokbro, Density-functional method for nonequilibrium electron transport, Phys. Rev. B **65**, 165401 (2002).

[56] G. Kresse and D. Joubert, From ultrasoft pseudopotentials to the projector augmented-wave method, Phys. Rev. B **59**, 1758 (1999).

[57] K. B. John, P. Perdew, and Matthias Ernzerhof, Generalized gradient approximation made simple, Phys. Rev. Lett. **78**, 1396 (1997).

[58] P. E. Blochl, Projector augmented-wave method, Phys. Rev. B **50**, 17953 (1994).

[59] R. Lake and S. Datta, Nonequilibrium Green's-function method applied to double-barrier resonant-tunneling diodes, Phys. Rev. B **45**, 6670 (1992).

[60] L. Kleinman and D. M. Bylander, Efficacious form for model pseudopotentials, Phys. Rev. Lett. **48**, 1425 (1982).

[61] See Supplemental Material at http://link.aps.org/supplemental/10.1103/PhysRevB.109.085201 for computational details, physical properties of CrSBr and CrI_3, comparisons between DFT+NEGF and quadratic perturbation theory, limitations of the photoexcitation method for generating spin-polarized current under gate voltage, band structure, photocurrent, and electrical transport properties of CrSBr. It also contains Refs. [4,11,12,14,17,18,23,25–60].

[62] S. Y. Huang, D. Qu, T. C. Chuang, C. C. Chiang, W. Lin, and C. L. Chien, Pure spin current phenomena, Appl. Phys. Lett. **117**, 190501 (2020).

[63] J. Yang, R. Quhe, S. Liu, Y. Peng, X. Sun, L. Zha, B. Wu, B. Shi, C. Yang, J. Shi, G. Tian, C. Wang, J. Lu, and J. Yang, Gate-tunable high magnetoresistance in monolayer Fe_3GeTe_2 spin valves, Phys. Chem. Chem. Phys. **22**, 25730 (2020).

[64] S. Pal, N. V. Sarath, K. S. Priya, and P. Murugavel, A review on ferroelectric systems for next generation photovoltaic applications, J. Phys. D: Appl. Phys. **55**, 283001 (2022).

[65] H. Tang, B. Shi, Y. Wang, C. Yang, S. Liu, Y. Li, R. Quhe, and J. Lu, Layer-dependent photoabsorption and photovoltaic effects in two-dimensional Bi_2O_2X (X = S, Se, and Te), Phys. Rev. Appl. **15**, 064037 (2021).

[66] S.-W. Cheong, SOS: Symmetry-operational similarity, npj Quantum Mater. **4**, 53 (2019).

[67] D. Xiao, M.-C. Chang, and Q. Niu, Berry phase effects on electronic properties, Rev. Mod. Phys. **82**, 1959 (2010).